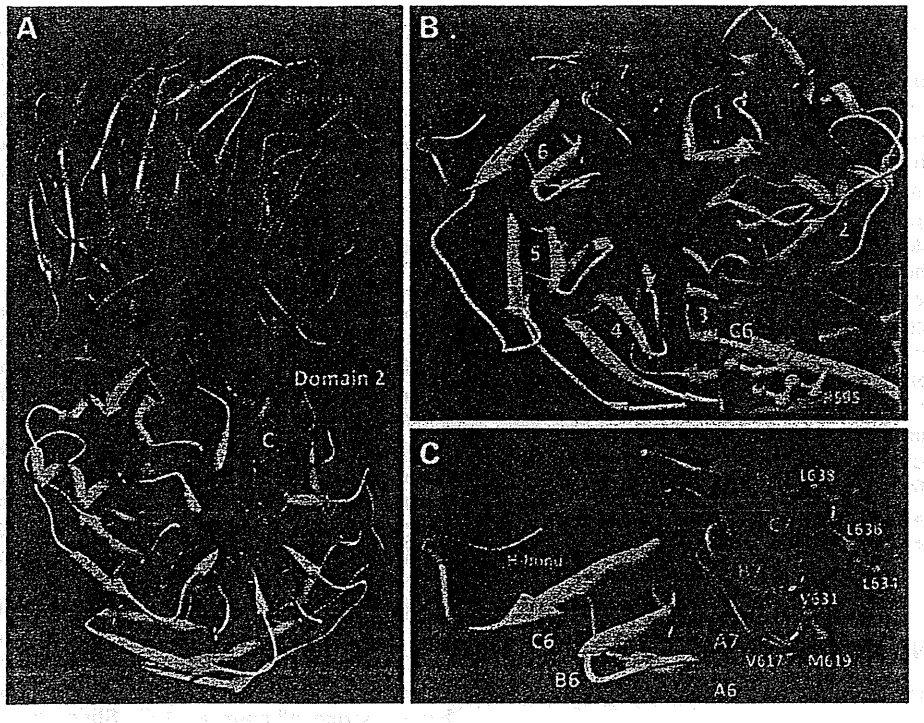

Figure 6. The WDR36 three-dimensional structure is obtained by homology modeling. The ribbon model with β-strands shown by arrows illustrates a proposed structure of WDR36 containing 14 WD40 repeats. N- and C-terminal domains with a seven-bladed β-propeller fold are shown by orange and cyan, respectively (A). In domain 2, individual blades with the WD40 structural motif are numbered from 1 to 7 (**B**). Similar to others, blade 6 is composed of an antiparallel β-sheet with the individual β-strands labeled from A6 to D6 (**C**). The individual β-strand D6 and the seventh blade of the domain 2 which correspond to mutations Del605–607 and Del601–640 are shown by blue and green, respectively. The Wt amino acid side chains that are important for the analysis of sequence variants are shown by ball and stick models. Hydrogen bonds are shown by cyan and orange lines. Interaction between residues R595 and D606 is revealed as an inset in (B). The missense mutation D606G cause the D606 side chain removal and breaks the single side chain–side chain hydrogen bond Asp606OD2–Arg595NH1. Amino acids are shown by a single letter code.

birth. In gross anatomical examination, the size and structural abnormalities of head, eye and gut, which occurred in zebrafish, were not observed in mice. The vulnerability of the retina in the mouse model may suggest a differential role of Wdr36 in the two species, perhaps through interaction with different retina-specific molecules. On the other hand, Skarie and Link (10) also showed the involvement of the p53 pathway and subsequent activation of p21 on the effects of the loss of Wdr36, suggesting that the p53 pathway may also have influenced the phenotype of our transgenic mice.

Overall, the adult Wdr36 transgenic mice with abnormal phenotype serve as the potential POAG model for future use. To date, a number of animal models for glaucoma have been established (12,18–24). Interestingly, the phenotypes of human glaucoma mutation-based mouse models including myocilin Y423H (20,17), optineurin E50K (12) and Wdr36 Del605-607 (Figs 2–4) all involve loss of peripheral RGCs accompanied by peripheral retinal degeneration. Herein, we raise the question, what are the reasons for peripheral retinal degeneration? Previous reports have indicated that mouse models of glaucoma follow similar natural courses of peripheral retinal degeneration (12,17–20). These findings suggest that all three mouse models share a common signaling pathway for RGC death and beyond, although the function of each protein is distinct. Wdr36 transgenic mouse will be useful in combination with other models to identify molecules responsible for this common pathway of RGC death.

Prediction by homology structure of Wdr36 was used to analyze three mutant variants D606G, Del605–607 and Del601–640, respectively (Fig. 1A). The missense change of aspartic acid to glycine at position 606 interrupts the side chain–side chain hydrogen bond Asp606OD2–Arg595NH1 without affecting other hydrogen bonds that stabilize interaction between C6 and D6 β-strands (Fig. 6B, inset). This minor change suggests that the mutation will show either no effect or an insignificant structural change in the stability of the protein with age that could potentially appear at a very slow rate. In contrast, the mutation Del605–607 removes residues from positions 605 to 607 corresponding to the β-strand D6 (Fig. 6A–C, blue). This results in interruption of five hydrogen bonds in Wdr36 structure, and might affect the stability of the 6th blade of domain 2 (Fig. 6B). Although it is difficult to make a definite conclusion, our modeling predicts that the polypeptide chain might still adopt a β-propeller conformation. Thus, domain 2 will continue to adopt a seven-blade β-propeller structure, suggesting that protein–protein interactions that involve residues after position 607 might be significantly perturbed because all interacting residues will be shifted by three residues from their original positions. Further, this could exclude the mutant variant from the

native pattern of protein–protein interactions, affecting biochemical pathways, and potentially leading to degenerative processes in the cell.

The Del601–640 construct removes β-strand D6 and seventh blade, shown by blue and green color, respectively, in Figure 6C. The deletion might dramatically affect a closure mechanism and hydrophobic interactions between blades 7 and 1 (Fig. 6C). As a result, this change significantly decreases protein stability by 'unlocking' the circular structure of the seventh-bladed β-propeller domain 2. The protein would definitely be expected to be misfolded, either forming insoluble aggregates or more likely be degraded in proteolytic pathways related to chaperone-mediated autophagy (25) or to the ubiquitin-proteasome system (26). If this hypothesis is correct, the mutant protein will be expressed but functionally inactive to influence the endogenous Wdr36.

Overall, the functional evidence in this study demonstrates an essential role for Wdr36 in mouse retina. These results will provide basis for future research to determine how WDR36 variants leads to POAG.

MATERIALS AND METHODS

Development of transgenic mouse over expressing Wt and mutant *Wdr36*

Full-length *Wdr36* cDNA was amplified from C57BL/6N mouse heart total RNA using DNA polymerase (PrimeSTAR HS DNA Polymerase, Takara, Tokyo, Japan) and cloned into pBluescript II KS(+) (Stratagene, La Jolla, CA, USA). D606G, and Del605–607, was introduced by site-directed mutagenesis (Quick Change XL Site Directed Mutagenesis Kit, Stratagene) in accordance with manufacturer's instructions. The primer sets used for mutagenesis of mouse *Wdr36* D606G and Del605–607 are 5′-CTGGGTGCCTTATCGGC TGCTTTTTGTTGGAC-3′, 5′-GTCCAACAAAAAGCAGCC GATAAGGCACCCAG-3′ and 5′-ACCTTCCTTCTGGGTGC CTTTTTTTGTTGGACTCAGCGCC-3′, 5′-GGCGCTGAGTC CAACAAAAAAAGGCACCCAGAAGGAAGGT-3′ respectively. Del601–640 was constructed by amplification of mouse *Wdr36* using primer set 5′-AATATTTCCCTCTATT CAGTTGT-3′ and 5′-AGGAAGGTCCCAAGTCCTAA-3′. Mutated cDNA was inserted into pCMV-Tag5 vector with chicken beta-actin promoter and CMV enhancer (pCAGGS) kindly provided by Dr Junichi Miyazaki (Osaka University). The Wt and mutant *Wdr36* cDNA fragment was released from the pBroad2 vector using Pac I. The *Wdr36* fragments were injected into pronuclear stage BDF1/C57BL6N embryos and transgenic mice were generated at PhoenixBio Co., Ltd (Utsunomiya, Japan). Offspring from 32 donor mice were screened for the transgene by isolating genomic DNA from tail biopsies followed by PCR. Primers used for PCR were: 5′-CAGAAACTCATCTCTGAAGAGGATCTGTAG-3′ and 5′-TTGTTCATGGCAGCCAGCATATGGCATATG-3′. All experimental data were obtained from 16-month-old Wt and mutant *Wdr36* transgenic mice. All the experiments using mice were performed in accordance with the Association for Research in Vision and Ophthalmology statement for the Use of Animals in Vision Research.

Light microscopic histopathology of the optic nerve

After euthanized, mouse eyes were dissected and immersed in Davidson solution fixative overnight at 4°C. The eyes were embedded in paraffin and sectioned at 5 μm thickness along the vertical meridian through the optic nerve head. After deparaffinization and rehydration, sections were H&E stained.

Immunohistochemistry

The eyes were sectioned at 5 μm thickness along the vertical meridian through the optic nerve head. After deparaffinization and rehydration, the tissue sections were treated with Target Retrieval Solution (Dako Cytomation, Denmark). For cryosections, after perfusion with 4% paraformaldehyde (PFA), the eye balls were dissected and immersed in OCT compound. The frozen eyes were sectioned at 10 μm thickness. The sections were incubated with blocking solution for 1 h followed by overnight incubation with primary antibody against myc-tag (1:100 dilution; Abcam, Cambridge, MA, USA), NeuN (1:100 dilution; Millipore, Billerica, MA, USA), calretinin (1:500 dilution; Sigma, Sigma-Aldrich, St Louis, MO, USA), tyrosine hydroxylase (1:100 dilution; Millipore), PKC α (1:500 dilution; Millipore), synaptophysin (1:500 dilution; Abcam) or ssDNA (1:500 dilution; Immuno-Biological Laboratories, Gunma, Japan) in phosphate-buffered saline (PBS) containing 1% bovine serum albumin at 4°C. Slides were washed in PBS and then incubated with Alexa 488 or Alexa 568 (1:500 dilution; Invitrogen, Carlsbad, CA, USA) conjugated secondary antibody and with 4′,6′-diamidino-2-phenylindole (DAPI) for nuclear staining for 1 h at room temperature. The stained tissues were examined using confocal fluorescence laser microscopy (Radiance 2000, Bio-Rad Laboratories, Hercules, CA, USA). As negative control of the immunohistochemical staining, the sections were incubated with blocking solution without primary antibody (data not shown).

Whole-mount immunostaining

The whole-mount immunostaining was performed essentially as described (23,27). Anterior parts were dissected from enucleated eyes. The posterior parts were fixed in 4% PFA/PBS for 2 h on ice and then incubated with the anti-SMI32 (1:200 dilution; Sternberger Monoclonals, Baltimore, MD, USA) and ssDNA antibody (1:500 dilution; Immuno-Biological Laboratories) for 7 days at 4°C. Slides were washed in PBS containing 0.1% Triton X-100 and then incubated with Alexa 488- or Alexa 568-conjugated secondary antibody (1:500 dilution; Invitrogen) and with DAPI for nuclear staining for 2 days at 4°C. The retinas were then mounted with Vectashield (Vector Laboratories, Burlingame, CA, USA) and evaluated on a confocal microscope.

Measurement of IOP

The average IOP for each genotype was determined. IOP was measured using an impact-rebound tonometer (Colonal Medical Supply, Franconia, NH, USA) for mice of each genotype as described previously (12). Using the rebound tonometer, we were able to measure IOP in awake and

non-sedated mice of various ages. Measurement of IOP was always performed in the morning between 10 am to noon. The numbers of mice successfully assessed for each genotype were 8 Wt mice and 32 mutant transgenic mice at 16 months after birth.

Primary culture of retinal ganglion cells

To evaluate axon outgrowth of primary RGC, Del605–607 mice were mated with Thy1-CFP transgenic mouse (28–30) [B6.Cg-Transgenic (Thy1-CFP) 23Jrs/J] obtained from Jackson Laboratory (Bar Harbor, ME, USA) to develop Del605–607/Thy1-CFP double transgenic mice. The double transgenic mice at postnatal 5 days were euthanized and the eye globes enucleated to dissect anterior parts from the eye. The retinas were dissociated by SUMITOMO nerve-cell culture system/dissociation solutions (Sumitomo Bakelite, Tokyo, Japan) and cultured in SUMITOMO culture medium for 7 days on poly-L-lysine-coated culture plates.

Molecular modeling of mouse Wdr36

The sequence of *Mus musculus* WD repeat domain 36 isoform 1, WDR36 (NP_001103485.1), was exported to protein homology/analogy recognition engine Phyre version 0.2 (http://www.sbg.bio.ic.ac.uk/~phyre/) where *C. elegans* homologue of yeast actin interacting protein 1 (UNC-78/AIP1) (PDB file: 1nr0) was identified as the top-score structural homolog hit and the structure of two consecutive WD40 domains was generated. Two structural domains in WDR36 protein sequence were confirmed with the program REPRO (31). Amino acid sequences of mice Wdr36 and *C. elegans* UNC-78/AIP1 were aligned with PROMALS3D (http://prodata.swmed.edu/promals3d). Individual WD40 repeat motifs and Utp21 C-terminal domain were localized using the modular architecture research tool SMART 6 available at http://smart.embl-heidelberg.de. The Wdr36-1nr0 alignment exported to Look version 3.5.2 to automatically generate homology models of mutant proteins with deletions Del605–607 and Del601–640 by the automatic segment matching method (32) followed by 500 cycles of energy minimization. The missense mutation Asp606Gly (D606G) was generated and refined by self-consistent ensemble optimization (33), which applies the statistical mechanical mean-force approximation iteratively to achieve the global energy minimum structure.

Statistical analysis

All data were expressed as the mean ± standard deviation (SD). Statistical differences were analyzed by the ANOVA or Student's *t*-test. $^*P < 0.05$ was considered statistically significant.

ACKNOWLEDGEMENTS

The authors thank Dr S. Zigler Jr for critical reading of the manuscript.

Conflict of Interest statement. None declared.

FUNDING

This research was supported in part by the grants to T.I. by the Japan Ministry of Health, Labour, and Welfare, the Japan Ministry of Education, Culture, Sports, Science and Technology and Grant-in-Aid for JSPS fellows for Z.-L.C. Funding to pay the Open Access Charge was provided by the Ministry of Health, Labour, and Welfare of Japan and the Ministry of Education, Culture, Sports, Science and Technology of Japan.

REFERENCES

1. Quigley, H.A. (1996) Number of people with glaucoma worldwide. *Br J Ophthalmol.*, **80**, 389–393.
2. Quigley, H.A. and Broman, A.T. (2006) The number of people with glaucoma world wide in 2010 and 2020. *Br. J. Ophthalmol.*, **90**, 262–267.
3. Stone, E.M., Fingert, J.H., Alward, W.L., Nguyen, T.D., Polansky, J.R., Sunden, S.L., Nishimura, D., Clark, A.F., Nystuen, A., Nichols, B.E. *et al.* (1997) Identification of a gene that causes primary open angle glaucoma. *Science*, **275**, 668–670.
4. Rezaie, T., Child, A., Hitchings, R., Brice, G., Miller, L., Coca-Prados, M., Heon, E., Krupin, T., Ritch, R., Kreutzer, D. *et al.* (2002) Adult-onset primary open-angle glaucoma caused by mutations in optineurin. *Science*, **295**, 1077–1079.
5. Monemi, S., Spaeth, G., DaSilva, A., Popinchalk, S., Ilitchev, E., Liebmann, J., Ritch, R., Heon, E., Crick, R.P., Child, A. *et al.* (2005) Identification of a novel adult-onset primary open-angle glaucoma (POAG) gene on 5q22.1. *Hum. Mol. Genet.*, **14**, 725–733.
6. Hauser, M.A., Allingham, R.R., Linkroum, K., Wang, J., LaRocque-Abramson, K., Figueiredo, D., Santiago-Turla, C., del Bono, E.A , Haines, J.L., Pericak-Vance, M.A. *et al.* (2006) Distribution of WDR36 DNA sequence variants in patients with primary open-angle glaucoma. *Invest. Ophthalmol. Vis. Sci.*, **47**, 2542–2546.
7. Weisschuh, N , Wolf, C., Wissinger, B. and Gramer, E. (2007) Variations in the WDR36 gene in German patients with normal tension glaucoma. *Mol. Vis* , **13**, 724–729.
8. Pasutto, F., Mardin, C.Y., Michels-Rautenstrauss, K., Weber, B.H , Sticht, H., Chavarria-Soley, G., Rautenstrauss, B., Kruse, F. and Reis, A. (2008) Profiling of WDR36 missense variants in German patients with glaucoma. *Invest. Ophthalmol Vis. Sci.*, **49**, 270–274.
9. Miyazawa, A., Fuse, N., Mengkegale, M., Ryu, M., Seimiya, M., Wada, Y and Nishida, K. (2007) Association between primary open-angle glaucoma and WDR36 DNA sequence variants in Japanese. *Mol. Vis.*, **13**, 1912–1919.
10. Skarie, J M. and Link, B.A. (2008) The primary open-angle glaucoma gene WDR36 functions in ribosomal RNA processing and interacts with the p53 stress-response pathway. *Hum. Mol. Genet.* **17**, 2474–2485.
11. Footz, T K., Johnson, J.L., Dubois, S., Boivin, N., Raymond, V. and Walter, M.A (2009) Glaucoma-associated WDR36 variants encode functional defects in a yeast model system. *Hum. Mol. Genet.* **18**, 1276–1287
12. Chi, Z.L , Akahori, M., Obazawa, M., Minami, M., Noda, T., Nakaya, N., Tomarev, S., Kawase, K., Yamamoto, T., Noda, S. *et al.* (2010) Overexpression of optineurin E50K disrupts Rab8 interaction and leads to a progressive retinal degeneration in mice. *Hum. Mol. Genet.*, **19**, 2606–2615.
13. Letunic, I., Doerks, T. and Bork, P. (2009) SMART 6: recent updates and new developments. *Nucleic Acids Res.*, **37**, D229–232.
14. Kelley, L.A. and Sternberg, M.J. (2009) Protein structure prediction on the Web: a case study using the Phyre server. *Nat. Protoc.*, **4**, 363–371
15. Mohri, K., Vorobiev, S., Fedorov, A.A., Almo, S.C. and Ono, S. (2004) Identification of functional residues on *Caenorhabditis elegans* actin-interacting protein 1 (UNC-78) for disassembly of actin depolymerizing factor/cofilin-bound actin filaments. *J. Biol. Chem* , **279**, 31697–31707.
16. Sondek, J , Bohm, A., Lambright, D.G., Hamm, H E. and Sigler, P.B. (1996) Crystal structure of a G-protein beta gamma dimer at 2.1A resolution. *Nature*, **379**, 369–374.
17. Zhou, Y., Grinchuk, O. and Tomarev, S.I. (2008) Transgenic mice expressing the Tyr437His mutant of human myocilin protein develop glaucoma. *Invest. Ophthalmol. Vis. Sci.*, **49**, 1932–1939.

18. Harada, T., Harada, C., Nakamura, K., Quah, H.M., Okumura, A., Namekata, K., Saeki, T., Aihara, M., Yoshida, H., Mitani, A. *et al.* (2007) The potential role of glutamate transporters in the pathogenesis of normal tension glaucoma. *J. Clin. Invest.*, **117**, 1763–1770.
19. John, S.W., Smith, R.S., Savinova, O.V., Hawes, N.L., Chang, B., Turnbull, D., Davisson, M., Roderick, T.H. and Heckenlively, J.R. (1998) Essential iris atrophy, pigment dispersion, and glaucoma in DBA/2J mice. *Invest Ophthalmol Vis Sci.*, **39**, 951–962.
20. Senatorov, V., Malyukova, I., Fariss, R., Wawrousek, E.F., Swaminathan, S., Sharan, S.K. and Tomarev, S. (2006) Expression of mutated mouse myocilin induces open-angle glaucoma in transgenic mice. *J. Neurosci.*, **26**, 11903–11914.
21. Chang, B., Smith, R.S., Hawes, N.L., Anderson, M.G., Zabaleta, A., Savinova, O., Roderick, T.H., Heckenlively, J.R., Davisson, M.T. and John, S.W. (1999) Interacting loci cause severe iris atrophy and glaucoma in DBA/2J mice. *Nat. Genet.*, **21**, 405–409.
22. Anderson, M.G., Smith, R.S., Hawes, N.L., Zabaleta, A., Chang, B., Wiggs, J.L. and John, S.W. (2002) Mutations in genes encoding melanosomal proteins cause pigmentary glaucoma in DBA/2J mice. *Nat. Genet.*, **30**, 81–85.
23. Jakobs, T.C., Libby, R.T., Ben, Y., John, S.W. and Masland, R.H. (2005) Retinal ganglion cell degeneration is topological but not cell type specific in DBA/2J mice. *J. Cell. Biol.*, **171**, 313–325.
24. Stoilov, I., Akarsu, A.N. and Sarfarazi, M. (1997) Identification of three different truncating mutations in cytochrome P4501B1 (CYP1B1) as the principal cause of primary congenital glaucoma (Buphthalmos) in families linked to the GLC3A locus on chromosome 2p21. *Hum. Mol. Genet.*, **6**, 641–647.
25. Kaushik, S. and Cuervo, A.M. (2008) Chaperone-mediated autophagy. *Methods. Mol. Biol.*, **445**, 227–244.
26. Goldberg, A.L. (2003) Protein degradation and protection against misfolded or damaged proteins. *Nature*, **426**, 895–899.
27. Howell, G.R., Libby, R.T., Jakobs, T.C., Smith, R.S., Phalan, F.C., Barter, J.W., Barbay, J.M., Marchant, J.K., Mahesh, N., Porciatti, V. *et al.* (2007) Axons of retinal ganglion cells are insulted in the optic nerve early in DBA/2J glaucoma. *J. Cell. Biol.*, **179**, 1523–1537.
28. Feng, G., Mellor, R.H., Bernstein, M., Keller-Peck, C., Nguyen, Q.T., Wallace, M., Nerbonne, J.M., Lichtman, J.W. and Sanes, J.R. (2000) Imaging neuronal subsets in transgenic mice expressing multiple spectral variants of GFP. *Neuron*, **28**, 41–51.
29. Vidal, M., Morris, R., Grosveld, F. and Spanopoulou, E. (1990) Tissue-specific control elements of the Thy-1 gene. *EMBO. J.*, **9**, 833–840.
30. Raymond, I.D., Vila, A., Huynh, U.C. and Brecha, N.C. (2008) Cyan fluorescent protein expression in ganglion and amacrine cells in a thy1-CFP transgenic mouse retina. *Mol. Vis.*, **14**, 1559–1574.
31. George, R.A. and Heringa, J. (2000) The REPRO server: finding protein internal sequence repeats through the web. *Trends. Biochem. Sci.*, **25**, 515–517.
32. Levitt, M. (1992) Accurate modeling of protein conformation by automatic segment matching. *J. Mol. Biol.*, **226**, 507–533.
33. Lee, C. (1994) Predicting protein mutant energetics by self-consistent ensemble optimization. *J. Mol. Biol.*, **236**, 918–939.

JBC Papers in Press. Published on November 8, 2010 as Manuscript M110.175810
The latest version is at http://www.jbc.org/cgi/doi/10.1074/jbc.M110.175810

PROCESSING OF OPTINEURIN IN NEURONAL CELLS

Xiang Shen[†], Hongyu Ying[†], Ye Qiu[†], Jeong-Seok Park[†], Rajalekshmy Shyam[†], Zai-Long Chi[§], Takeshi Iwata[§], and Beatrice Y.J.T. Yue[†]

From [†]the Department of Ophthalmology and Visual Sciences, University of Illinois at Chicago College of Medicine, Chicago, Illinois, USA and [§]National Institute of Sensory Organs, National Hospital Organization Tokyo Medical Center, Tokyo, Japan

Running head: Processing of Optineurin

Address correspondence to: Beatrice Yue, PhD, Department of Ophthalmology and Visual Sciences, University of Illinois at Chicago, 1855 West Taylor Street, Chicago, IL 60612. Fax: 312-996-7773; E-mail: beatyue@uic.edu

Optineurin is a gene linked to amyotrophic lateral sclerosis, Paget's disease of bone, and glaucoma, a major blinding disease. Mutations such as Glu50Lys (E50K) were identified in glaucoma patients. We investigated herein the involvement of ubiquitin-proteasome pathway (UPP) and autophagy, two major routes for protein clearance, in processing of optineurin in a retinal ganglion cell (RGC) model line RGC5 and neuronal PC12 cells. It was found that the endogenous optineurin level in neuronal cells was increased by treatment of proteasomal inhibitors, but not by autophagic and lysosomal inhibitors. Multiple bands immunoreactive to anti-ubiquitin were seen in the optineurin pull down, indicating that optineurin was ubiquitinated. In cells overexpressing wild type and E50K optineurin, the level of proteasome regulatory β5 subunit (PSMB5, indicative of proteasome activity) was reduced while that for autophagy marker microtubule-associated protein 1 light chain 3 (LC3) was enhanced compared to controls. Autophagosome formation was detected by electron microscopy. The foci formed after optineurin transfection were increased upon treatment of an autophagic inhibitor, but were decreased by treatment of an inducer, rapamycin. The level of optineurin-triggered apoptosis was moreover reduced by rapamycin. The current study thus provides compelling evidence that in normal homeostatic situation, the turnover of endogenous optineurin involves mainly UPP. When optineurin is upregulated or mutated, the UPP function is compromised and autophagy comes into play. A decreased PSMB5 level and an induced autophagy were also demonstrated *in vivo* in RGCs of E50K transgenic mice, validating and making relevant the *in vitro* findings.

Glaucoma is one of the leading causes of irreversible blindness worldwide (1) characterized by progressive loss of retinal ganglion cells (RGCs) and axons, and distinctive cupping of the optic nerve head. The most common form of this disease, primary open angle glaucoma (POAG), is genetically heterogeneous, caused by several susceptibility genes and perhaps also environmental factors (1-4). Currently, a total of 14 chromosomal loci, designated as GLC1A to GLC1N, have been linked to POAG. Three candidate genes identified so far include myocilin (GLC1A), optineurin (GLC1E), and WD40-repeat36 (GLC1G) (1-3). Among them, optineurin is linked principally to normal pressure or normal tension glaucoma (NTG), a subtype of POAG (5). Optineurin mutations were noted to vary with ethnic background (6). The Glu50Lys (E50K) mutation, found in Caucasian and Hispanic populations (6), seems to be associated with a more progressive and severe disease in NTG patients (7). Very recently, optineurin has also been linked to amyotrophic lateral sclerosis (ALS, 8) and Paget's disease of bone (9).

The human optineurin gene codes for a 577-amino acid protein that contains multiple coiled-coil domains and a C-terminal zinc finger (10). The optineurin protein from different species has high amino acid homology (11) and the amino acid 50 glutamic acid residue is conserved in mouse, rat, chicken and cow (12). Optineurin is ubiquitously expressed in non-ocular tissues such as the heart and brain (10) and in ocular tissues including the retina, trabecular meshwork, and non-pigmented ciliary epithelium (9). In the retina, RGCs are immunolabeled with a high intensity (12, 13).

Optineurin shares a 53% amino acid homology with NEMO (NF-κB essential modulator) and was identified as a NEMO-related protein (14). Recently, optineurin has been shown to be a negative regulator of NF-κB (15). Like NEMO, optineurin has a polyubiquitin binding region in the sequence and it binds K-63 linked polyubiquitinated chains (16). Optineurin has in addition been demonstrated to interact with itself to form homo-hexamers (17). It also interacts with proteins including myosin VI, Rab8, and transferrin receptor. Super molecular complexes are detected and granular structures termed foci are formed when optineurin is overexpressed or E50K mutated (17, 18).

Proper processing of cellular proteins is of vital importance. In eukaryotic cells, the ubiquitin-proteasome pathway (UPP) and autophagy are two major routes for protein clearance (19-21). Proteasomes predominantly degrade, in a specific manner, short-lived nuclear and cytosolic proteins. The bulk degradation of long-lived cytoplasmic proteins or organelles is mediated largely by autophagy. Proteins can also be degraded through the autophagy-independent endosome-lysosome system.

Protein degradation via UPP is a temporally controlled and tightly regulated process that involves covalent linking of a single or multiple molecules of ubiquitin to a target protein. The ubiquitinated protein is then marked for degradation by the multi-subunit 26S proteasome complex. The proteolytic core of the complex, the 20S proteasome, contains multiple peptidase activities that include chymotrypsin-like, postglutamyl peptidase or caspase-like and trypsin-like activities. Ubiquitination has been shown to be a pivotal player in regulating a host of cellular processes including cell cycle control, differentiation and quality control (22). It is important not only in cellular homeostasis in tissues/organs including the nervous system but also in degradation of misfolded and aberrant proteins.

Autophagy is an evolutionally conserved mechanism responsible for the nonselective bulk degradation of long-lived proteins and cytoplasmic recycling of organelles during development, tissue homeostasis, and environmental stress such as starvation or amino acid depletion (23, 24). There are three types of autophagy: macroautophagy, chaperone-mediated autophagy, and microautophagy. Among them, macroautophagy (hereafter referred to as autophagy) is the one mediated by the organelle termed autophagosome. Chaperone-mediated autophagy involves the direct translocation of cytosolic proteins across the lysosomal membrane, which requires protein unfolding by chaperone proteins. Microautophagy involves inward invagination of lysosomal membrane, which delivers a small portion of cytoplasm into the lysosomal lumen.

Autophagy begins with the formation of double-membrane bounded autophagosomes (25-27) which then fuse with lysosomes and/or endosomes to form autolysosomes. The contents of autolysosomes are finally degraded by acidic lysosomal hydrolases and the degraded products are transported back to the cytoplasm. Autophagy has been shown to play a role in organelle turnover, cancer cell biology, aging, and neurodegenerative disorders (23, 28-30).

In the present investigation, we determined the involvement of UPP and autophagy in processing of the endogenous optineurin in RGC5 cells, a neuronal cell type recently shown to be of mouse origin (31) and an established model for RGCs (31, 32), as well as neuronal rat adrenal pheochromocytoma PC12 cells (33). The processing of overexpressed wild type optineurin and E50K mutant protein was also studied to test the hypothesis that similar to other neurodegenerative diseases, UPP function is compromised and autophagy is induced with elevated level or mutation of aggregate-prone optineurin.

EXPERIMENTAL PROCEDURES

Cell lines - RGC5 cells were obtained from the University of Illinois at Chicago, Ophthalmology departmental core facility, deposited by Dr. Paul Knepper (34) and originally from Dr. Neeraj Agarwal, North Texas Health Science Center, Fort Worth, TX (31). PC12 cells were purchased from American Type Culture Collection (Masnassas, VA, USA). The cells were cultured in serum-containing complete medium as previously described (18, 35).

In some experiments, RGC5 cells were treated with tumor necrosis factor-α (TNF-α, 100 ng/ml, R & D Systems, Minneapolis, MN) or interferon-γ (IFN-γ, 20 ng/ml, R & D Systems) for 24 h. Both have been shown to elevate the level of optineurin (14, 15, 36). Tetracycline regulated (Tet-on) wild type optineurin ($OPTN_{WT}$)-green fluorescence protein (GFP) inducible stable RGC5 cell line was established as previously described (17). Tet-on inducible E50K optineurin ($OPTN_{E50K}$)-GFP RGC5 cell line was in addition created following the same procedures and strategies. The only exception was that the $OPTN_{WT}$-GFP fragment was replaced with $OPTN_{E50K}$-GFP during the first cloning step (17). The cells were maintained in DMEM complete medium with 10% Tet system certified fetal bovine serum (Clontech, Mountain View, CA), essential and nonessential amino acids, and antibiotics. To induce expression of $OPTN_{WT}$-GFP and $OPTN_{E50K}$-GFP, cells were treated for 16 h with doxycycline (DOX, 1 μg/ml) (Clontech) in DMEM complete medium.

DNA constructs – Optineurin expression vectors pTarget-$OPTN_{WT}$, pTarget-FLAG-$OPTN_{WT}$, p$OPTN_{WT}$-EGFP, p$OPTN_{WT}$-DsRed, as well as pTarget-$OPTN_{E50K}$, p$OPTN_{E50K}$-GFP, and p$OPTN_{E50K}$-DsRed were constructed as previously described (18). Transient transfection was performed using lipofectamine LTX and Plus reagent (Invitrogen,) for 20-48 h according to manufacturer's protocol.

Western blotting - To examine the effects of various inhibitors on levels of the endogenous optineurin, RGC5 and PC12 cells in 6-well plates (300,000 cells/well) were treated for 16 h with vehicle dimethylsulfoxide (DMSO) or H_2O, proteasomal inhibitors lactacystin (LCT, 1 μM) and epoxomicin (5 μM), autophagic inhibitor 3-methyladenine (3-MA, 5 mM), lysosomal inhibitor NH_4Cl (1 mM), or autophagic inducer rapamycin (2 μM). LCT is a proteasomal inhibitor but it also inhibits enzymes such as cathepsin A. Epoxomicin on the other hand is a potent and specific proteasomal inhibitor. 3-MA inhibits class III phosphatidylinositol 3-kinase (PI3K) that is essential for autophagosome formation, as well as other classes of PI3K. It is used as an effective and selective drug to inhibit autophagy degradation. At 5 mM, it has no detectable effects on other proteolytic pathways (27). NH_4Cl is a lysosomotropic weak base that blocks the intralysosomal degradation of macromolecules via inhibition of the acidification of the endosome-lysosome system. It does not affect enzyme activities.

The cells were lysed with lysis buffer (250 mM NaCl, 50 mM Tris/HCl, pH7.5, 5 mM EDTA, 0.5% Nonidet P40) supplemented with protease inhibitor cocktail (Sigma, St. Louis, MO). Protein concentration was determined by bicinchoninic acid protein assay (Pierce, Rockford, IL). Total cell lysate was then subjected to sodium dodecyl sulfate-polyacrylamide gel electrophoresis (SDS-PAGE) under reducing conditions. The proteins were transferred to nitrocellulose membrane and the level of endogenous optineurin was assessed by Western blotting using rabbit anti-C-terminal-optineurin (Cayman Chemical, 1:1000). The membrane was also immunoblotted with polyclonal anti-glyceraldehyde 3-phosphate dehydrogenase (GAPDH, 1:5000, Trevigen, Gaithersburg, MD) for loading control. Immunoreactive protein bands were detected by chemiluminescence using SuperSignal Substrate (Pierce). Densitometry was performed. The band intensity of the endogenous optineurin was normalized to that of GAPDH.

For levels of proteasome regulatory β5 subunit (PSMB5) that is responsible for the chymotrypsin-like activity of the proteasome (37) and an established autophagic marker microtubule-associated protein 1 light chain 3 (LC3) (25), RGC5 and PC12 cells were transfected for 20 h with pTarget empty vector, pTarget-$OPTN_{WT}$ or pTarget-$OPTN_{E50K}$. Total lysate was subject to SDS-PAGE and levels of PSMB5, LC3, and GAPDH were assessed by immunoblotting using polyclonal rabbit anti-PSMB5 (Abcam, Cambridge, MA, 1:1000), monoclonal anti-LC3 (1:1000, Enzo Life Sciences, Farmingdale, NY), and rabbit anti-GAPDH (1:5000).

Immunoprecipitation (IP) - Lysates from RGC5 cells untreated or treated with 1 μM LCT for 16 h were immunoblotted using polyclonal anti-optineurin or monoclonal anti-ubiquitin (1:2000, Biomol, Enzo Life Sciences). Lysates were also immunoprecipitated with rabbit anti-C-terminal-optineurin or rabbit normal IgG (negative control) using the Catch and Release kit (Millipore, Billerica, MA). The proteins pulled down were subjected to SDS-PAGE under reducing

conditions. The ubiquitinated proteins were detected with mouse anti-ubiquitin antibody.

Fluorescence microscopy and immunohistochemistry - RGC5 and PC12 cells were transfected for 20 h with pEGFP-N1 (mock control), pOPTN$_{WT}$-EGFP or pOPTN$_{E50K}$-EGFP. The cells were subsequently treated for 24 or 48 h with autophagic inhibitor 3-MA (5 mM) or overnight with rapamycin (2 μM). The cells were fixed and images were acquired.

For immunofluorescence, the cells were fixed after transfection or treatments, and single or double stained with rabbit anti-optineurin (1:100), rabbit anti-PSMB5 (1:100), or rabbit (MBL International, Woburn, MA) or mouse anti-LC3 (1:100). FITC-goat anti-rabbit IgG, Cy3-goat anti-rabbit IgG, or Cy3-goat anti-mouse IgG (Jackson ImmunoResearch, West Grove, PA; 1:200) was used as the secondary antibody. The slides were mounted in Vectashield (Vector Laboratories, Burlingame, CA) with 4',6-diamidino-2-phenylindole (DAPI).

Photography was carried out using a 63× oil objective on an Axioscope (Carl Zeiss MicroImaging, Thornwood, NY) with the aid of Metamorph software (Molecular Devices, Downingtown, PA). In some experiments, confocal microscopic analysis was performed on a Leica SP2 confocal system (Leica Microsystems, Bannockburn, IL) using the Leica confocal software following sequential scanning to minimize the bleed through.

GFP^u reporter assay – To visualize the change of proteasome activity by optineurin transfection, a GFP^u reporter plasmid (American Type Culture Collection) was used. It is a designer reporter consisting of a short 16-amino acid degron CL1 (a substrate for UPP) fused to the C-terminus of GFP (38, 39). For GFP^u reporter assay, cells co-transfected with GFP^u and pDsRed empty vector (mock control), pOPTN$_{WT}$-DsRed, or pOPTN$_{E50K}$-DsRed for 24 h were examined by confocal microscopy. Images were captured after sequential scanning and the intensity of green fluorescence in at least 60 red-fluorescent transfected cells was quantified.

Transmission electron microscopy: RGC5 cells transfected for 20 h to express GFP, OPTN$_{WT}$-GFP, or OPTN$_{E50K}$-GFP were fixed in 2.5% glutaraldehyde, 2% paraformaldehyde in sodium cacodylate buffer, pH 7.4, postfixed in osmium tetroxide, and embedded in Epon resin. Ultra thin sections (70 nm) were counterstained with uranyl acetate and lead citrate and observed under a JEOL JEM-1220 transmission electron microscope.

For immunogold experiments, inducible cells without or with DOX treatment were fixed at 4°C in 4% paraformaldehyde, 0.1% glutaraldehyde, in phosphate buffered saline, pH 7.4 for 2 h, and sequentially dehydrated in ethanol solutions and embedded in LR-White resin. Sections (90 nm) mounted on 200-mesh nickel grids were blocked and then incubated with polyclonal anti-GFP (1:100, for wild type or E50K optineurin-GFP) and monoclonal anti-LC3 (1:50). The secondary antibodies used were 25-nm colloid gold-conjugated goat anti-rabbit IgG and 10-nm gold conjugated goat anti-mouse IgG (1:25, Jackson ImmunoResearch).

Apoptosis assay - Apoptosis was evaluated by the BIOMOL CV-caspase 3/7 detection kit (Enzo Life Sciences) that utilizes the fluorophore, cresyl violet, coupled to the C-terminus of the optimal tetrapeptide recognition sequences for caspase 3/7, DEVD [CR(DEVD)$_2$]. Cleavage of the target sequences by activated enzymes yields red fluorescence throughout the cell, indicative of apoptotic activity. RGC5 and PC12 cells on glass chamber slides were transiently transfected for 48 h to express GFP, or wild type or E50K optineurin-GFP. Cells were incubated with CR(DEVD)$_2$ for 60 min after treatment with rapamycin for 30 h. The untreated control did not receive rapamycin treatment. The slides were mounted in Vectashield with DAPI which stained nuclei of all transfected and non-transfected cells.

The total number of DAPI-stained transfected cells (green) and the number of CR(DEVD)$_2$-stained transfectants (displaying both green and red fluorescence) in 20 of randomly selected 10x fields were counted (40). The percentage of caspase 3/7-positive apoptotic cells in approximately 100 transfectants (number of green and red cells/number of green only cells) was calculated. The experiments were repeated three times. Statistical analysis was performed using Student's *t* tests.

Transgenic mice - The E50K transgenic mice were generated as previously described (41). All the experiments using mice were performed in

accordance with the Association for Research in Vision and Ophthalmology statement for the Use of Animals in Vision Research.

The IOP of the transgenic mice was measured using an impact-rebound tonometer (Colonal Medical Supply, Franconia, NH) and optical interferometry tonometer (FISO Technologies, Quebec, Canada). Optic disk imaging and light microscopic histopathologic examination of the optic nerve were carried out. Paraffin sections of retinal tissues were prepared for TUNEL assay (39). Sections (5 μm) from 12-month-old normal and transgenic mice were deparaffinized, and stained in parallel with hematoxylin and eosin, monoclonal anti-TUJ1 (anti-βIII-tubulin, 1:400, Covance, Princeton, NJ) to highlight RGC layer (42), or polyclonal anti-optineurin (1:100), anti-PSMB5 (1:250), or anti-LC3 (1:200). Qdot 655 goat anti-mouse or rabbit IgG (1:100, Invitrogen, Carlsbad, CA) was used as the secondary antibody. The slides were mounted in Vectashield, examined under Axioscope, and photographed. In some experiments, sections from 4- and 8-month-old mice were prepared and immunostained with anti-optineurin, anti-PSMB5 and anti-LC3. For EM, 12-month-old mouse eyes were fixed in 2.5% glutaraldehyde, 2% paraformaldehyde in phosphate buffer. The retinas were dissected out and the tissues were postfixed in 1% osmium tetroxide, sequentially dehydrated, and embedded in Spurr's resin. Thin sections (90 nm) were cut and stained for examination under JEOL 1200 EX transmission electron microscope.

RESULTS

Endogenous optineurin level in RGC5 and PC12 cells. Cells were treated with proteasomal, autophagic and lysosomal inhibitors. As can be seen in Fig. 1, the endogenous optineurin level in both RGC5 and PC12 cells was increased by 2-3 fold upon treatment with proteasomal inhibitors, LCT and expoxomicin, but only by 1.1-1.4 fold with autophagic and lysosomal inhibitors. Rapamycin, an autophagic inducer, did not alter the optineurin level, supporting the 3-MA results that autophagy has a minimal role in the processing of the endogenous optineuirn.

Optineurin is ubiquitinated. Lysates from RGC5 cells were immunoprobed for optineurin and ubiquitin. Consistent with results from Fig. 1, the level of optineurin was increased upon treatment of LCT. Also seen were higher molecular weight bands with stronger intensities in LCT-treated samples (Fig. 2A, left panel). Meanwhile, LCT treatment, as anticipated, resulted in an enhanced level of total ubiquitinated proteins in cell lysates (Fig. 2A, right panel).

Lysates were in addition immunoprecipitated with polyclonal anti-optineurin and immunoprobed with monoclonal anti-ubiquitin. Multiple bands immunoreactive to anti-ubiquitin were observed in the immunoprecipitated protein pool, indicating that the endogenous optineurin in RGC5 cells was ubiquitinated (Fig. 2B, left panel). The intensity of the ubiquitin-positive bands was enhanced by prior LCT treatment. The same blot was also probed with anti-optineurin to verify the IP procedure (Fig. 2B, right panel).

Optineurin foci formation. After transfection, the overexpressed optineurin-GFP fusion protein distributed diffusely in the cytoplasm of RGC5 and PC12 cells with dots or granular structures observed most notably near the nucleus (Fig. 3). These structures, referred to as foci, were also observed previously in human retinal pigment epithelial (RPE) and trabecular meshwork cells (18). Foci formation in addition was noted in cells after transfection to overexpress E50K optineurin-GFP. The number and the size of the E50K-GFP foci were greater than those of the wild type (Fig. 3), as was reported previously in RPE cells (18).

Reduced proteasome activity in optineurin overexpressing cells. RGC5 cells transfected for 20 h to express wild type and E50K optineurin-GFP were immunostained for PSMB5 as an indication of proteasome activity (37). The staining intensity in green optineurin-overexpressing RGC5 cells was much reduced compared to mock controls and non-transfected cells (Fig. 4A). Western blot analyses indicated that the PSMB5 protein level was decreased (0.36 ± 0.10 and 0.30 ± 0.14 respectively, $n = 3$, $P < 0.002$) as the optineurin level was increased by 8 to 10 fold upon transfection of pTarget-wild type and E50K optineurin (Fig. 4B). Similar alterations were also observed in PC 12 cells (data not shown).

The cells were subsequently co-transfected with $pOPTN_{WT}$-DsRed and GFP^u reporter plasmid. This ubiquitin proteasome system reporter has been shown to be degraded in mammalian cells in an ubiquitin-dependent manner (38, 39). Proteasomal inhibitors such as LCT, but not other protease inhibitors, increased the steady state level of GFP^u (39). Its fluorescence readout and dependence on ubiquitin thus make GFP^u a simple and reliable tool (30). Results shown in Figs. 4C and D revealed that the GFP^u green fluorescence was increased, indicating a lowered proteasome activity in cells transfected with $pOPTN_{WT}$-DsRed compared to those of DsRed control and non-transfected cells. A decreased proteasome activity was also seen in cells transfected with $pOPTN_{E50K}$-DsRed (Fig. 4C).

Induction of autophagy in optineurin overexpressing cells. Following optineurin transfection, RGC5 (Fig. 5) and PC12 (data not shown) cells were stained for autophagic marker, LC3. The intensity of LC3 staining in optineurin transfected green cells was found stronger than that seen in mock controls and non-transfected cells (Fig. 5A). Partial colocalization between optineurin foci and LC3 staining was observed.

LC3 exists in two forms. LC3-I (18 kDa) is cytosolic and LC3-II (16 kDa) is lipidated (conjugated to phosphatidylethanolamine) that inserts into the membrane. The amount of LC3-II is correlated with the extent of autophagosome formation and increasing levels of LC3-II on immunoblots have been used to document induction of autophagy (27). In RGC5 cells, the level of LC3 protein, especially the active LC3-II form, was found substantially increased (2.4 ± 0.4 and 2.7 ± 0.5 respectively, $n = 5$, $P < 0.002$) by Western blotting upon overexpression of wild type and E50K optineurin (Fig. 5B).

In separate experiments, RGC5 cells were treated with TNF-α and IFN-γ for 24 h. The optineurin level was increased by approximately 2 fold, as was reported previously (14, 15, 36). Foci formation was not apparent but the PSMB5 level was found reduced by 40 to 60% while the LC3-II level was elevated by 1.9 to 2.5 fold (Fig. 6). Similar PSMB5 and LC3 alterations were also observed in inducible cell lines when wild type and E50K optineurin-GFP levels were induced by 10-12 fold and foci were formed upon DOX treatment (data not shown). It is of note that the overexpressed or upregulated optineurin levels seen in Figs 4-6 are not the expression levels, but rather the stationary state levels set by expression and degradation. The resulting level depends not only on the translational increase, but also on the maximum ability of the cell to degrade the excess proteins. This indicates that the transient overexpression might be much higher than 10X, but could be regulated somewhat by the autophagic degradation process.

Furthermore, electron dense as well as electron-light double- or multiple-membrane autophagosome- and autolysosome-like structures or vesicles (43, 44) were prominently observed by electron microscopy in RGC5 cells after optineurin transfection (Fig. 7A, a-c). These structures were rarely detected in GFP control (Fig. 7Ad) and non-transfected (data not shown) cells.

Autophagosome-like structures were also observed in inducible wild type (data not shown)- and E50K (Fig. 7B, a and b)-GFP-expressing cells following DOX induction, but not in non-induced cells (Fig. 7Bb, insert). Immunogold studies showed co-localization of E50K optineurin-GFP and LC3 in autophagosome-like structures (Fig. 7B, c and d).

Optineurin foci formation is regulated by autophagy. RGC5 (Fig. 8, A and B) and PC12 (data not shown) cells transfected with $pOPTN_{WT}$-GFP and/or $pOPTN_{E50K}$-GFP for 20 h were treated with 3-MA or rapamycin for 24 or 48 h. The 3-MA treated cells showed more optineurin wild type foci formation compared with the untreated controls (Fig. 8A) and the foci enhancement was more dramatically seen at the 48-h time point. The rapamycin treated cells on the other hand, showed less foci formation compared with untreated group in both $pOPTN_{WT}$-GFP- and $pOPTN_{E50K}$-GFP-transfectants (Fig. 8B), suggesting that the overexpressed optineurin was cleared, at least in part, via the autophagy pathway.

Rapamycin treatment reduces the level of apoptosis induced by overexpressed optineurin. RGC5 (Fig. 8C) and PC12 (data not shown) cells were transiently transfected to express GFP alone, wild type or E50K optineurin-GFP followed by treatment of rapamycin. Images were captured and the percentage of cells that exhibited activated caspase 3/7 enzymes, representing apoptotic activity, in the transfected population was determined. Results indicated that without the

rapamycin treatment, the percentage of caspase 3/7-positive cells in total wild type and E50K optineurin-GFP-overexpressing transfectants was increased by approximately 1.8 to 2.5 fold ($P < 0.008$) compared to that in pEGFP-N1-transfected mock controls (Fig. 8C). After the rapamycin treatment, the level of apoptosis in optineurin transfectants was declined to within the control limits (Fig. 8C).

Transgenic E50K mouse. The E50K mouse is transgenic, not a knock-in mouse. The transgene was expressed using the chicken β-actin promoter (pCAGGS) with CMV enhancer. The copy number for the mutant gene was approximately 12 to 14 per mouse (41). While the distribution remained similar, the overall optineurin expression was higher in the retina of E50K transgenic mice compared with the endogenous optineurin expression. The RGC loss and retinal thinning were seen 12 month after birth in the transgenic mice. By 16 months, approximately 43% of the retinal thickness and approximately 20% of RGC numbers were reduced (41). Excavation of the optic nerve head was also observed. Apoptotic RGCs were detected in 16 month or older E50K mice. The average IOP reading for mutant mice was in the normal range of 15 ± 1 mmHg for all examined ages (41).

Tissue sections from 12-month-old E50K transgenic mice displayed a fainter staining of PMSB5 but a stronger staining of LC3 in RGCs compared with those from control littermate mice (Fig. 9B). Staining with anti-optineurin also yielded a higher intensity in the transgenic tissues as expected (Fig. 9B). The enhanced LC3 and reduced PSMB5 staining was also observed in sections from the 4- and 8-month-old transgenic mice (data not shown). Interestingly, no pathology was apparent in the former mice while retinal thickness appeared to be somewhat reduced in the latter.

The staining results in 12-month-old E50K transgenic and normal mice were confirmed by Western blotting of retinal extracts (Fig. 9C). By electron microscopy, autophagosome-like structures were demonstrated in RGCs of E50K transgenic eyes (Fig. 9D). Quantification analyses indicated that the structures were found in 22 of 33 RGCs examined in transgenic mouse sections, but only in 1 of 23 RGCs in controls.

DISCUSSION

In eukaryotic cells, the ubiquitin-proteasome and autophagy pathways are two major routes for protein clearance (19-21). The present study demonstrates that proteasomal inhibition led to an increase in the endogenous optineurin level in neuronal RGC5 and PC12 cells (Fig. 1). On the other hand, autophagic and lysosomal inhibition as well as autophagic activation had little effects. The UPP thus appeared to be the major pathway for endogenous optineurin processing. Autophagy and lysosomes had a rather minor, if any, role. Supporting this conclusion, the endogenous optineurin in RGC5 cells was found ubiquitinated (Fig. 2). UPP has been shown to be the pathway that degrades in a specific manner short-lived proteins. The involvement of UPP is therefore consistent with our finding that the half life of the endogenous optineurin is approximately 8 h (17). Ubiquitination of the endogenous optineurin also agrees with a previous observation that ^{35}S-labeled, *in vitro*-translated optineurin binds to ubiquitin and is ubiquintinated (16).

Our study further indicates that upon optineurin overexpression or mutation, the proteasome activity in neuronal cells is decreased (Fig. 4) while autophagy is induced. The induction of autophagy is evidenced by an increased immunostaining (Fig. 5A) for an established autophagic marker LC3 (25), an increased protein level of LC3-II (Fig. 5B), the lipidated form of LC3 that inserts into the membrane and correlates with the appearance of LC3-positive autophagosomes (27, 45-47), plus the detection of autophagosome- and autolysosome-like structures in transfected cells (Fig. 6). The overexpressed wild type and E50K optineurins appeared to be processed largely through autophagy, as autophagic activator rapamycin diminishes, while the inhibitor 3-MA augments the foci formation (Fig. 8, A and B).

A decrease in the PSMB5 level and an increase in the LC3 level were similarly observed in cells treated with TNF-α and IFN-γ (Fig. 6) as well as in inducible cell lines (data not shown). Such *in vitro* changes were likewise observed *in vivo* in E50K transgenic mice. The E50K-overexpressing mice developed phenotype that mimicked the clinical features of NTG patients including neuropathy of the optic disc and

degeneration of the RGCs without an increased IOP (41). This mouse line thus appears to be the first NTG mouse model. It is notable that the intensity changes of PSMB5 and LC3 staining, although not dramatic, were readily visible (Fig. 9B). The protein level changes in the 12-month-old E50K mice were confirmed by Western blotting (Fig. 9C). Autophagosome- and autolysosome-like structures were also observed in the E50K specimens (Fig. 9D).

It has been documented that when a cytosolic protein is aggregate-prone, it becomes a poor proteasome substrate. One example is α-synuclein, a protein of unknown function and a major component of Lewy bodies (aggregates) observed in Parkinson's diesease. Mutations of α-synuclein are known to cause autosomal dominant, early-onset Parkinson's disease. Previous studies have disclosed that both UPP and autophagy are routes for α-synuclein degradation and that while soluble α-synuclein is cleared by proteasome, the aggregated protein or mutants are preferentially cleared by autophagy (30, 47).

The optineurin degradation hence parallels that described for α-synuclein. The endogenous optineurin seems to be degraded chiefly through the ubiquitin pathway. When optineurin is upregulated or mutated in neuronal cells, autophagy becomes involved (Figs. 5-7).

The optineurin overexpression characteristics bear similarities to those seen in neurodegenerative diseases including Alzheimer's and Huntington's (20, 48, 49). After transfection with wild type or E50K optineurin, the optineurin foci are observed to distribute in perinuclear region in proximity to the Golgi complex (17, 18, 40). Following precedent of those described for aggresomes, inclusion bodies or Lewy bodies, the optineurin foci are formed in a microtubule-dependent manner (17, 18). They appear to be LC3-positive (Fig. 5A). Also, the proteasome function is impaired (Fig. 4, C and D) as was seen in neurodegenerative diseases (49-51). In addition, overexpression of both wild type and E50K optineurin leads to apoptosis in cultured cells (40) and the toxicity can be rescued by rapamycin treatment (Fig. 8C). These analogies further underline that glaucoma shares common features with neurodegenerative diseases (52-54).

The role or significance of the foci observed in glaucoma is at present unclear. Interestingly, the roles of inclusion bodies and aggresomes formed in other neurodegenerative diseases are also not clear. As summarized in a number of reviews (21, 26, 55, 56), the inclusion bodies and aggresomes may play protective role by sequestering toxic, misfolded protein species and providing the cells with an opportunity of delayed protein degradation. They may also inactivate the proteasome and mediate cytotoxicity. Inhibition of proteasome is believed to induce autophagy, which serves as a default mechanism for degradation of the accumulated abnormal proteins. However, when the autophagic clearance system reaches saturation, unable to eliminate the excess proteins, dysregulation or defection may occur, contributing to apoptosis and pathology (26). Supporting this notion, diffuse and abnormal proteins accumulate and aggregate to form inclusions which can disrupt the neural system in Atg5 (autophagy-related gene 5) deficient mice (57). Also, the protein accumulation and neurodegenerative phenotype could be reverted by activation of the autophagy pathway with a gene therapy approach (58) or infusion of rapamycin (55). It is suggested that there may exist a threshold as a point of divergence between physiological and pathological autophagy (59) and both the physiological and pathological roles of autophagy remain as critically important areas for investigations. Furthermore, inhibition of proteasome function has also been shown to trigger apoptosis (60) depending on cell types and conditions. Defects in the UPP may drive human pathologies including neurodegenerative diseases (30) although there have been controversies that still await further clarification (61).

A similar scenario may take place in optineurin-related glaucoma. In this context, it is intriguing that a persistent accumulation of autophagosomes was observed in a recent study (62) in the rat optic nerve following an optic nerve crush injury. The autophagy observed, possibly related to the lesion-induced calcium influx, was thought to be the major pathophysiological mechanism contributing to the ensuing axonal degeneration. It is also of interest that very recently mutations of optineurin are reported to be involved in the pathogenesis of ALS (8). While the role of foci in pathology remains to be precisely defined, an ALS case with the E478G optineurin mutation did show optineurin- and

ubiquitin-positive cytoplasmic inclusions. Optineurin in addition is linked to Paget's disease (9), a condition characterized by focal increases in bone turnover. The osteoclasts in affected bone also contain intranuclear inclusion bodies (63).

There is growing evidence that ubiquitin may be involved in "selective" autophagy (21, 64). It has been shown that ubiquitin binding receptors such as p62 are required in the process of autophagic clearance of protein aggregates (61, 64). By binding simultaneouly to ubiquitin and autophagosome-associated ubiquitin-like LC3, the receptors mediate docking of ubiquitinated protein aggregates to the autophagosome for selective degradation. Optineurin is ubiquitinated, whether its aggregates are processed through the "selective" autophagy process is currently unknown.

Taken together, the current study provides compelling evidence that in normal homeostatic situation, the turnover of endogenous optineurin involves mainly UPP. When optineurin is upregulated or mutated, the UPP function is compromised and autophagy comes into play. A decreased PSMB5 level and an induced autophagy were also demonstrated *in vivo* in RGCs of E50K transgenic mice, validating and making relevant the *in vitro* findings.

Optineurin and E50K mutant have been shown to inhibit NF-κB activation (8, 15). Studies from our laboratory reveal that the interaction with Rab8 and transferrin receptor is stronger with E50K mutant than the wild type optineurin. The mutant also produces a more prominent foci formation (17, 18), more severe fragmentation of the Golgi complex (18), and a higher level of apoptosis (40) than overexpression of the wild type optineurin. Representing a gain-of-function mutation, E50K in addition impairs more dramatically the transferrin trafficking (65). Based on these observations, we surmise that the defective trafficking, deregulated NF-κB signaling, along with fragmentation of the Golgi complex and increased apoptosis may be the underlying bases how E50K optineurin mutation renders the patients predisposed to the glaucoma pathology. Autophagy, on the other hand, may not be a primary factor in the disease development. This pathway may simply be induced initially as a protective response with build-up of the aggregate-prone mutant protein. Autophagy may contribute to the demise of the cells only when the build-up exceeds the capacity, exacerbating then the disease condition.

It is additionally noteworthy that while the E50K findings have pathologic significance, the wild type optineurin overexpression results may also be of physiologic relevance. Optineurin, for example, is known to be upregulated by proinflammatory cytokines TNF-α (14, 36) and IFN (14). Its expression may be heightened to set off adverse consequences upon acute or chronic inflammation and infection. Increases of TNF-α in the retina and the optic nerve head have been associated with glaucomatous conditions (66).

Knowledge of the degradation pathways acting on optineurin can help in design of novel therapeutic strategies (30). For example, proteasome activity can be promoted by overexpression of proteasome subunit or molecular chaperones and autophagy can be upregulated by rapamycin (30), rapamycin plus lithium combination (67), or small molecule autophagy enhancers (68). Future studies will be focused on this translational aspect.

REFERENCES

1. Allingham, R. R., Liu, Y., and Rhee, D. J. (2009) *Exp. Eye Res.* **88**, 837-844
2. Wiggs, J. L. (2007) *Arch. Ophthalmol.* **125**, 30-37
3. Kwon, Y. H., Fingert, J. H., Kuehn, M. H., and Alward, W. L. M. (2009) *N. Engl. J. Med.* **360**, 1113-1124
4. Wang, N., Chintala, S. K., Fini, M. E., and Schuman, J. S. (2001) *Nat. Med.* **7**, 304-309
5. Rezaie, T., Child, A., Hitchings, R., Brice, G., Miller, L., Coca-Prados, M., Heon, E., Krupin, T., Ritch, R., Kreutzer, D., Crick, R. P., and Sarfarazi, M. (2002) *Science* **295**, 1077-1079

6. Hauser, M. A., Sena, D. F., Flor, J., Walter, J., Auguste, J., Larocque-Abramson, K., Graham, F., Delbono, E., Haines, J. L., Pericak-Vance, M. A., Allingham, R. R., and Wiggs, J. L. (2006) *J. Glaucoma* **15**, 358-363
7. Aung, T., Rezaie, T., Okada, K., Viswanathan, A. C., Child, A. H., Brice, G., Bhattacharya, S. S., Lehmann, O. J., Sarfarazi, M., and Hitchings, R. A. (2005) *Invest. Ophthalmol. Vis. Sci.* **46**, 2816-2822
8. Maruyama, H., Morino, H., Ito, H., Izumi, Y., Kato, H., Watanabe, Y., Kinoshita, Y, Kamada, M., Nodera H., Suzuki, H., Komure, O., Matsuura, S, Kobatake, K., Morimoto, N., Abe K, Suzuki, N., Aoki, M., Kawata, A., Hirai, T., Kato, T., Ogasawara, K., Hirano, A., Takumi, T., Kusaka, H., Hagiwara, K., Kaji, R., and Kawakami, H. (2010) *Nature* **465**, 223-226
9. Albagha, O. M. E., Visconti, M. R., Alonso, N., Langston, A. L., Cundy, T., Dargie, R., Dunlop, M. G., Fraser, W. D., Hooper, M. J., Isaia, G., Nicholson, G. C., del Pino Montes, J., Gonzalez-Sarmiento, R., di Stefano, M., Tenesa, A., Walsh, J. P., and Ralston, S. H. (2010) *Nat. Genet.* **42**, 520-524
10. Li, Y., Kang, J., and Horwitz, M. S. (1998) *Mol. Cell. Biol.* **18**, 1601-1610
11. Rezaie, T., and Sarfarazi, M. (2005) *Genomics* **85**, 131-138
12. Kroeber, M., Ohlmann, A., Russell, P., and Tamm, E. R. (2006) *Exp. Eye Res.* **82**, 1075-1085
13. De Marco, N., Buono, M., Troise, F., and Diez-Roux, G. (2006) *J. Biol. Chem.* **281**, 16147-16156
14. Schwamborn, K., Weil, R., Courtois, G., Whiteside, S. T., and Israel, A. (2000) *J. Biol. Chem.* **275**, 22780-22789
15. Sudhakar, C., Nagabhushana, A., Jain, N., and Swarup, G. (2009) *PLoS ONE* **4**, e5114
16. Zhu, G., Wu, C. J., Zhao, Y., and Ashwell, J. D. (2007) *Curr. Biol.* **17**, 1438-1443
17. Ying, H., Shen, X., Park, B. C., and Yue, B. Y. J. T. (2010) *PLoS One* **5**, e9168
18. Park, B. C., Shen, X., Samaraweera, M., and Yue, B. Y. J. T. (2006) *Am. J. Pathol.* **169**, 1976-1989
19. Glickman, M. H., and Ciechanover, A. (2002) *Physiol. Rev.* **82**, 373-428
20. McCray, B. A., and Taylor, J. P. (2008) *Neurosignals* **16**, 75-84
21. Kirkin, V., McEwan, D. G., Novak, I., and Dikic, I. (2009) *Mol. Cell* **34**, 259-269
22. Mukhopadhyay, D., and Riexman, H. (2007) *Science* **315**, 201-205
23. Mizushima, N. (2007) *Genes Dev.* **21**, 2861-2873
24. Meijer, A. J., and Codogno, P. (2009) *Crit. Rev. Clin. Lab. Sci.* **46**, 210-240
25. Eskelinen, E. (2005) *Autophagy* **1**, 1-10
26. Bao, X. H., Naomoto, Y., Hao, H. F., Watanabe, N., Sakurama, K., Noma, K., Motoki, T., Tomono, Y., Fukazawa, T., Shirakawa, Y., Yamatsuji, T., Matsuoka, J., and Takaoka, M. (2010) *Int. J. Mol. Med.* **25**, 493-503
27. Mizushima, N., Yoshimori, T., and Levine, B. (2010) *Cell* **140**, 313-326
28. Levine, B., and Kroeme, G. (2008) *Cell* **732**, 27-42
29. Mizushima, N., Levine, B., Cuervo, M., and Kilonsky, D. J. (2008) *Nature* **451**, 1069-1075
30. Rubinsztein, D. C. (2006) *Nature* **443**, 780-786
31. Krishnamoorthy, R. R., Agarwal, P., Prasanna, G., Vopat, K., Lambert, W., Sheedlo, H. J., Pang, I. H., Shade, D., Wordinger, R. J., Yorio, T., Clark, A. F., and Agarwal, N. (2001) *Brain Res. Mol. Brain Res.* **86**, 1-12
32. Van Bergen, N. J., Wood, J. P., Chidlow, G., Trounce, I. A., Casson, R. J., Ju, W. K., Weinreb, R. N., and Crowston, J. (2009) *Invest. Ophthalmol. Vis. Sci.* **50**, 4267-4272
33. Greene, L. A., Tischler, A. S. (1976) *Proc. Natl. Acad. Sci. USA* **73**, 2424-2428
34. Choi, J., Miller, A. M., Nolan, M. J., Yue, B. Y., Thotz, S. T., Clark, A. F., Agarwal, N., and Knepper, P. A. (2005) *Invest. Ophthalmol. Vis. Sci.* **46**, 214-222
35. Park, B. C., Tibudan, M., Samaraweera, M., Shen, X., and Yue, B. Y. J. T. (2007) *Genes Cells* **12**, 969-979
36. Vittitow, J. L., and Borras, T. (2002) *Biochem. Biophys. Res. Commun.* **298**, 67-74

37. Caballero, M., Liton, P. B., Challa, P., Epstein, D. L., and Gonzalez, P. (2004) *Biochem. Biophys. Res. Commun.* **323**, 1048-1054
38. Bence, N. F., Sampat, R. M., and Kopito, R. R. (2001) *Science* **292**, 1552-1555
39. Bence, N. F., Bennet, E. J., and Kopito, R. R. (2005) *Methods Enzymol.* **399**, 481-490
40. Koga T., Shen, X., Qiu Y, Park BC, Shyam R, and Yue, B. Y. J. T. (2010) *Am. J. Pathol.* **176**, 343-352
41. Chi, Z. L., Akahori, M., Obazawa, M., Minami, M., Noda, T., Nakaya, N., Tomarev, S., Kawase, K., Yamamoto, T., Noda, S., Sasaoka, M., Shimazaki, A., Takada, Y., Iwata, T. (2010) *Hum. Mol. Genet.* **19**, 2606-2615
42. Huang, Y., Li, Z., van Rooijen, N., Wang, N., Pang, C. P., and Cui, Q. (2007) *Exp. Eye Res.* **85**, 659-666
43. Eskelinen, E.-L. (2008) *Autophagy* **4**, 257-260
44. Martinez-Vicente, M., Talloczy, Z., Wong, E., Tang, G., Koga, H., Kaushik, S., de Vries, R., Arias, E., Harris, S., Sulzer, D., and Cuervo, A. M. (2010) *Nat. Neurosci.***13**, 567-576
45. Klinosky, D. J., Cuervo, A. M., and Seglen, P. O. (2007) *Autophagy* **3**, 181-206
46. Mizushima, N., and Yoshimori, T. (2007) *Autophagy* **3**, 542-545
47. Webb, J. L., Ravikumar, B., Atkins, J., Skepper, J. N., and Rubinsztein, D. C. (2003) *J. Biol. Chem.***278**, 25009–25013
48. Pan, T., Kondo, S., Le, W., and Jankovic, J. (2008) *Brain* **131**, 1969-1978
49. Bence, N. F., Sampat, R. M., and Kopito, R. R. (2001) *Science* **292**, 1552-1555
50. Mayer, R. J. (2003) *Drugs News Perspect.* **16**, 103-108
51. Ross, C. A., and Pickart, C. M. (2004) *Trends Cell Biol.* **14**, 703-711
52. McKinnon, S. J. (2003) *Front Biosci.* **8**, s1140-1156
53. Gupta, N., and Yucel, Y. H. (2007) *Curr. Opin. Ophthalmol.* **18**, 110-114
54. Normando, E. M., Coxon, K. M., Guo, L., and Cordeiro, M. F. (2009) *Exp. Eye Res.* **89**, 446-447
55. Garcia-Arencibia, M., Hochfeld, W. E., Toh, P. P. C., and Rubinsztein, D. C. (2010) *Semin .Cell Dev. Biol.* **21**, 691-698
56. Glick, D., Barth, S., and Macleod, K. F. (2010) *J. Pathol.* **221**, 3-12
57. Hara, T., Nakamura, K., Matsui, M., Yamamoto, A., Nakahara, Y., Suzuki-Migishima, R., Yokoyama, M., Mishima, K., Saito, I., Okano, H., and Mizushima, N. (2006) *Nature* **441**, 885-889
58. Spencer, B., Potkar, R., Trejo, M., Rockenstein, E., Patrick, C., Gindi, R., Adame, A., Wyss-Coray, T., and Masliah, E. (2009) *J. Neurosci.* **29**, 13578-13588
59. Cherra, S. J., Dagda, R. K., and Chu, C. T. (2010) *Neuropathol. Applied Neurobiol.* **36**, 125-132
60. Jana, N. R., Zemskov, E. A., Wang, G., and Nukina, N. (2001) *Hum. Mol. Genet.* **10**, 1049-1059
61. Matsuda, N., and Tanaka, K. (2010) *J. Alzheimer's Dis.* **19**, 1-9
62. Knoferle, J., Koch, J. C.,Ostendorf, T., Michel, U., Planchamp, V., Vutova, P., Tonges, L., Stadelmann, C., Bruck, W., Bahr, M., and Lingor, P. (2010) *Proc. Natl. Acad. Sci.* **107**, 6064-6069
63. Ralston, S. H. (2008) *Bone* **43**, 819-825
64. Wong, E., and Cuervo, A. M. (2010) *Nat. Neurosci.* **13**, 805-811
65. Park, B. C., Ying, H., Shen, X., Park, J. S., Qiu, Y., Shyam, R., and Yue, B. Y. J. T. (2010) *PLos One* **5**, e11547
66. Tezel, G. (2008) *Prog. Brain Res.* **173**, 409-421
67. Sarkar, S., Krishna, G., Imarisio, S., Saiki, S., O'Kane, C. J., and Rubinsztein, D. C. (2008) *Hum. Mol. Genet.* **17**, 170-178
68. Renna, M., Jimenez-Sanchez, M., Sarkar, S., and Rubinsztein, D. C. (2010) *J. Biol. Chem.* **285**, 11061-11067

FOOTNOTES

* We thank Ruth Zelkha for expert imaging and Jack Gibbons, Division of Biological Sciences for immunogold electron microscopy. This work was supported by National Eye Institute, National Institutes of Health, Grants EY018828, EY005628, EY003890 (to B.Y.J.T.Y.), and Core Grant EY01792, and the Ministry of Health, Labor, and Welfare, and the Ministry of Education, Culture, Sports, Science and Technology of Japan (to T.I.). The costs of publication of this article were defrayed in part by the payment of page charges.

The abbreviations used are: ALS, amyotrophic lateral sclerosis; Atg5, autophagy-related gene 5; NH_4Cl, ammonium chloride; DAPI, 4',6-diamidino-2-phenylindole; DMSO, dimethylsulfoxide; DOX, doxycycline; GAPDH, glyceraldehyde 3-phosphate dehydrogenase; E50K, Glu50Lys; Epoxo, epoxomicin; GFP, green fluorescence protein; H & E, hematoxylin and eosin; His, histidine; IFN-γ, interferon-γ; IB, immunoblotting; IP, immunoprecipitation; kb, kilobases; kDa, kilodaltons; LC3, microtubule-associated protein 1 light chain 3; LCT, lactacystin; 3-MA, 3-methyladenine; NC, negative control; NEMO, NF-κB essential modulator; NTG, normal tension glaucoma; OPTN, optineurin; PCR, polymerase chain reaction; PI3K, phosphatidylinositol 3-kinase; POAG, primary open angle glaucoma; PSMB5, proteasome regulatory β5 subunit; RGC, retinal ganglion cell; RPE cell, retinal pigment epithelial cell; Rapa, rapamycin; SDS-PAGE, sodium dodecyl sulfate-polyacrylamide gel electrophoresis; TNF-α, tumor necrosis factor-α; TUNEL, terminal deoxynucleotidyl transferase dUTP nick end labeling; WT, wild type.

FIGURE LEGENDS

Fig. 1. Effects of proteasomal, autophagic, and lysosomal inhibitors on levels of the endogenous optineurin (OPTN) in RGC5 (**A**) and PC12 (**B**) cells. Cells were treated for 16 h with vehicle DMSO or H_2O, or proteasomal (lactacystin [LCT] and epoxomicin [Epoxo]), autophagic (3-MA), or lysosomal (NH_4Cl) inhibitors. In a separate experiment, cells were also treated with rapamycin (Rapa) or vehicle (H_2O) for 16 h. Proteins (25 μg) in cell lysates were immunoblotted with anti-optineurin or anti-glyceraldehyde 3-phosphate dehydrogenase (GAPDH). Densitometry was performed. The optineurin/GAPDH relative to the DMSO or H_2O control ratios are presented.

Fig. 2. **A.** Total lysates from RGC5 cells without or with treatment of lactacystin (LCT, 1 μM, 16 h) were immunoblotted (IB) with polyclonal anti-optineurin (anti-OPTN, left panel), anti-GAPDH, or monoclonal anti-ubiquitin (anti-Ub, right panel). **B.** Total lysates from RGC5 cells without or with the LCT treatment were immunoprecipitated (IP) with rabbit anti-OPTN polyclonal antibody or normal rabbit IgG (as a negative control, NC) followed by immunoblotting (IB) with mouse anti-Ub monoclonal antibody. Optineurin pull down by rabbit anti-OPTN, but not the rabbit IgG control, showed multiple bands immunoreactive to anti-Ub (left panel). The intensity of the ubiquitin-positive bands was enhanced by prior LCT treatment. The same blot was also probed with anti-OPTN (right panel) to verify the IP procedure.*, the 74-kDa optineurin band.

Fig. 3. Foci formation in RGC5 (**A**) and PC12 (**B**) cells after 20 h-transfection with pEGFP-N1 (mock control), $pOPTN_{WT}$-GFP, and $pOPTN_{E50K}$-GFP to express GFP, wild type and E50K optineurin-GFP. The optineurin-GFP fusion proteins distributed diffusely in the cytoplasm of RGC5 and PC12 cells with dots or granular structures (arrows) observed most notably near the nucleus. These structures are referred to as foci. Scale bar, 10 μm.

Fig. 4. **A.** PSMB5 immunostaining (in red) in RGC5 cells. The cells were transfected for 20 h to express GFP, $OPTN_{WT}$-GFP, or $OPTN_{E50K}$-GFP. All transfectants displayed green fluorescence. Note a

reduced PSMB5 staining intensity in optineurin-GFP-expressing green cells compared with GFP-expressing or non-transfected cells. The reduction was more striking with the E50K mutation than the wild type. Scale bar, 10 μm. **B.** Western blotting for PSMB5 protein level. RGC5 cells were transfected for 20 h with pTarget, pTarget-$OPTN_{WT}$, or pTarget-$OPTN_{E50K}$. Total lysate was subject to SDS-PAGE and immunoblotting (IB) using polyclonal rabbit anti-optineurin, anti-PSMB5 or anti-GAPDH. The optineurin (OPTN) level, normalized to that of GAPDH, was increased by 9.8 and 7.5 fold, respectively, after wild type and E50K optineurin-GFP transfection. The PSMB5/GAPDH relative to the GFP control ratios are presented. Similar results were also obtained with PC12 cells (data not shown). **C.** GFP^u reporter assay. RGC5 cells were co-transfected with GFP^u and pDsRed, $pOPTN_{WT}$-DsRed, or $pOPTN_{E50K}$-DsRed for 20 h. The transfected cells displaying both green and red fluorescence were examined by confocal sequential analyses. The loss of GFP^u green fluorescence is an indication of proteasome activity. The fluorescence intensity from GFP^u is thus inversely correlated to the proteasome activity. Scale bar, 10 μm. **D.** The intensity of green fluorescence from GFP^u in red fluorescent transfected cells was quantified. Results are presented as mean ± SEM ($n \geq 60$) per transfected cells. The higher the value, the lower is the proteasome activity. *, $P < 0.0001$ compared to DsRed controls.

Fig. 5. **A.** LC3 immunostaining in transfected RGC5 cells. The cells transfected for 20 h to express GFP, $OPTN_{WT}$-GFP, or $OPTN_{E50K}$-GFP were stained with rabbit anti-LC3 in red. The GFP and LC3 merged images are presented. Note an increased LC3 staining in optineurin transfected green cells. The optineurin foci (green) and LC3 (red) were colocalized partially in the perinuclear region in yellow. Bar, 10 μm. **B.** Western blotting for LC3 protein level. RGC5 cells were transfected for 20 h with pTarget, pTarget-$OPTN_{WT}$, or pTarget-$OPTN_{E50K}$. Total lysate was subject to SDS-PAGE and immunoblotting (IB) using rabbit anti-optineurin, mouse anti-LC3 or rabbit anti-GAPDH. Both LC3-I and LC3-II protein bands were detected. The optineurin (OPTN) level, normalized to that of GAPDH, was increased by 11.5 and 12.3 fold respectively after wild type and E50K optineurin transfection. The LC3/GAPDH relative to the pTarget control ratios are presented. Similar alterations were also observed in PC12 cells (data not shown).

Fig. 6. **A.** Optineurin and PSMB5 immunostaining in RGC5 cells. The cells were treated with TNF-α (100 ng/ml) or IFN-γ (20 ng/ml) for 24 h and were stained with polyclonal rabbit anti-optineurin in green or polyclonal rabbit anti-PSMB5 in red. The micrographs shown for optineurin and PSMB5 staining were from different specimens. **B.** Optineurin and PSMB5 immunostaining in RGC5 cells. The cells were treated with TNF-α or IFN-γ as in **A**. The specimens were double stained with rabbit anti-optineurin in green and monoclonal anti-LC3 in red. Cells from the same fields are shown for both optineurin and LC3 staining. Scale bar, 10 μm. **C.** Immunoblotting (IB) using anti-optineurin (OPTN), anti-PSMB5, anti-LC3, and anti-GAPDH in cells untreated (lane 1, control), or treated with TNF-α (lane 2) or IFN-γ (lane 3) for 24 h. Note that the 18-kDa LC3-I band was barely visible. Only the 16-kDa LC3-II band is shown. As stated earlier, LC3 exists in two forms. LC3-I is cytosolic and LC3-II is lipidated and membrane bound. The amount of LC3-II is correlated with the extent of autophagosome formation and an increasing level of LC3-II on immunoblots signals autophagy induction. Bar graph depicts the relative intensities (levels) of OPTN, PSMB5, and LC3 compared to untreated controls after normalization to the GAPDH level.

Fig. 7. **A.** Autophagosome- and autolysosome-like structures in optineurin wild type (**a** and **b**)- and E50K-GFP (**c**)-expressing RGC5 cells. By electron microscopy, the electron dense, organelle-sequestrating, double- or multi-membrane structures with diameter averaged between 400-600 nm were not observed in GFP-expressing mock transfected cells (**d**). Scale bar, 5 μm in **a**, 0.5 μm in **b** and **c**, and 1 μm in **d**. **B.** Autophagosome- and autolysosome-like structures are observed in inducible RGC5 cells after DOX induction to express E50K optineurin-GFP (**a-d**). A lower magnification micrograph is shown in **a** demonstrating those structures in cytoplasm of several cells. Co-localization of optineurin-GFP (25 nm gold particles) and LC3 (10 nm gold particles) in those structures is seen by immunogold labeling

experiments (**c** and **d**). The autophagosome- and autolysosome-like structures are barely detected in non-induced controls (insert in **b**). Scale bar, 1 μm in **a**, 0.5 μm in **b**, and 0.2 μm in insert, **c** and **d**.

Fig. 8. Effects of 3-MA and rapamycin on optineurin foci formation. **A.** RGC5 cells transfected for 20 h with $pOPTN_{WT}$-GFP were untreated (control) or treated for 24 or 48 h with 3-MA (5 mM), an autophagy inhibitor. Optineurin foci formation was visualized under a Zeiss fluorescence microscope. Note an increased foci formation in 3-MA treated cells. **B.** RGC5 cells transfected with $pOPTN_{WT}$-GFP and $pOPTN_{E50K}$-GFP were treated for 20 h with rapapmycin (2 μM), an autophagy inducer. Note a reduction in foci formation with rapamycin treatment. Scale bar, 10 μm. Similar results were also obtained with PC12 cells (data not shown). **C.** Percentage of caspase 3/7-positive apoptotic cells in transfected RCG5 cells. The cells transfected for 48 h to express GFP (mock control), wild type optineurin-GFP (OPTN-GFP) and E50K optineurin-GFP (E50K-GFP) were examined by a caspase 3/7 detection kit. One set of cells was treated with 2 μM of rapamycin [(+) Rapamycin] for the last 30 h and another was untreated [(-) Rapamycin]. Images in 20 of 10× fields were captured and cell counting was performed to determine the total number of transfected cells (green) and the number of caspase 3/7-positive transfectants (green and red). Percentage of caspase 3/7-positive apoptotic transfected cells was calculated. Results from 3 independent experiments are shown in mean ± SEM. *, $P < 0.008$ compared to GFP controls. Similar patterns were also observed with PC12 cells (data not shown).

Fig. 9. **A.** Retinal sections from 12-month-old E50K transgenic and normal littermate mice were stained with monoclonal anti-TUJ1 (in red) to highlight the RGC layer, and with hematoxylin and eosin (H & E) to demonstrate retinal layers. GCL, ganglion cell layer; IPL, inner plexiform layer; INL, inner nuclear layer; OPL, outer plexiform layer; ONL, outer nuclear layer; POS, photoreceptor outer segments; and RPE, retinal pigment epithelium. Note that the retinal thickness is reduced in E50K transgenic specimen compared to normal control. Scale bar, 50 μm. **B.** Retinal sections from normal and E50K mice were stained in parallel with polyclonal anti-optineurin, anti-PSMB5, or anti-LC3 (all in red). All staining was done using the same antibody concentrations with identical exposure times. As RGCs are the focus of the study, staining in RGCs and the adjacent inner plexiform layer is shown in a higher magnification. Negative controls (NC) in which serial sections were stained only with secondary antibodies (for both monoclonal and polyclonal primary antibodies) are shown in inserts. There was a modest decrease in staining intensity of PSMB5 but an increase in LC3 staining in RGC layer in transgenic sections compared to normal controls. The optineurin staining was also enhanced in the transgenic mouse. Scale bar, 50 μm. **C.** Western blotting for optineurin (OPTN), PSMB5, LC3, and GAPDH levels in retinal extracts from normal (lane 1) or E50K (lane 2) mice. Note that for LC3, the 18-kDa LC3-I band was extremely faint. Only the 16-kDa LC3-II band is shown. Bar graphs, representing results from 3 experiments, depict the levels of optineurin, PSMB5, and LC3 relative to normals after normalization to the GAPDH level. *, $P < 0.0053$ compared to normals. **D.** Autophagosome- and autolysosome-like structures are observed in RGCs of E50K mouse (left and middle panels), but are rarely seen in normal littermates (right panel). Bar, 1 μm in the left panel, and 0.5 μm in middle and right panels.

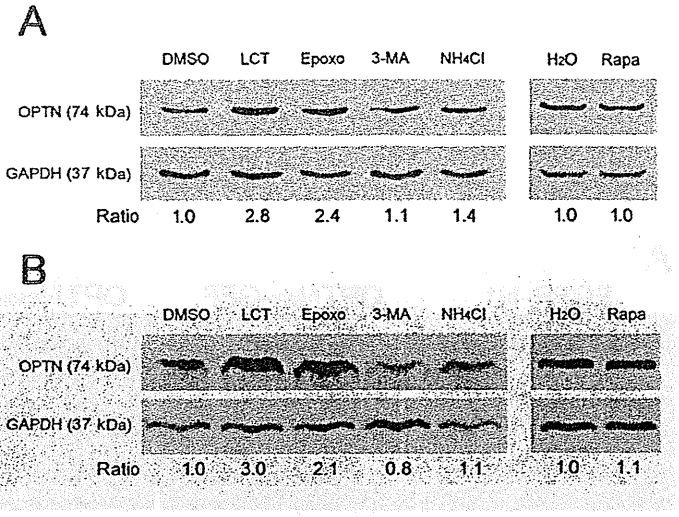

Figure 1

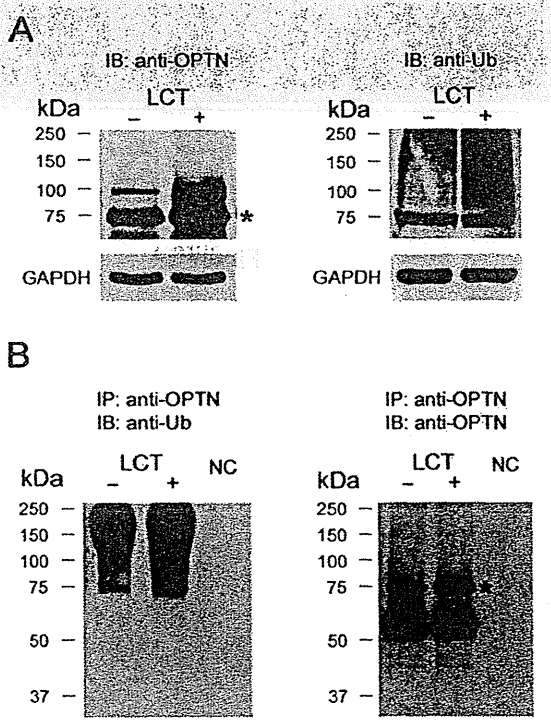

Figure 2

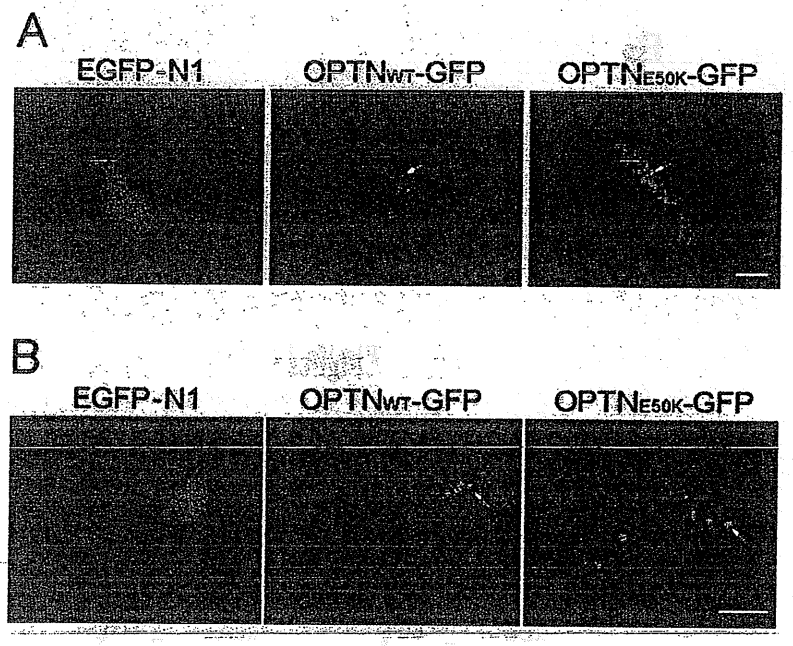
A
EGFP-N1
OPTNWT-GFP
OPTNE50K-GFP
B
EGFP-N1
OPTNWT-GFP
OPTNE50K-GFP

Figure 3